## Title
Cloud Forming Potential of Aerosol from Light-duty Gasoline Direct Injection Vehicles



## Authors
Fofie, Emmanuel A
Karavalakis, Georgios
Asa-Awuku, Akua

## Publication Date
2017-12-01

# Cloud Forming Potential of Aerosol from Light-duty Gasoline Direct Injection Vehicles

December 2017

A Research Report from the National Center for Sustainable Transportation

Emmanuel A. Fofie, University of California, Riverside
Georgios Karavalakis, University of California, Riverside
Akua Asa-Awuku, University of California, Riverside

National Center for Sustainable Transportation

UC RIVERSIDE UNIVERSITY OF CALIFORNIA

## About the National Center for Sustainable Transportation

The National Center for Sustainable Transportation is a consortium of leading universities committed to advancing an environmentally sustainable transportation system through cutting-edge research, direct policy engagement, and education of our future leaders. Consortium members include: University of California, Davis; University of California, Riverside; University of Southern California; California State University, Long Beach; Georgia Institute of Technology; and University of Vermont. More information can be found at: ncst.ucdavis.edu.

## U.S. Department of Transportation (USDOT) Disclaimer



## Acknowledgments

This study was funded by a grant from the National Center for Sustainable Transportation (NCST), supported by USDOT through the University Transportation Centers program. The authors would like to thank the NCST and USDOT for their support of university-based research in transportation, and especially for the funding provided in support of this project. The authors would like to thank the team at CE-CERT Vehicle Emissions Laboratory – Mark Villela, Edward O'Neil, Patrick Roth, and Jiancheng Yang.

NCST

# Cloud Forming Potential of Aerosol from Light-duty Gasoline Direct Injection Vehicles

A National Center for Sustainable Transportation Research Report

December 2017

**Emmanuel Fofie,** CE-CERT*, University of California, Riverside

**Georgios Karavalakis,** CE-CERT, University of California, Riverside

**Akua Asa-Awuku,** CE-CERT, University of California, Riverside

* College of Engineering – Center for Environmental Research and Technology

NCST

[page left intentionally blank]

# TABLE OF CONTENTS

# Cloud Forming Potential of Aerosol from Light-duty Gasoline Direct Injection Vehicles

## EXECUTIVE SUMMARY

In this study, we evaluate the hygroscopicity and droplet kinetics of fresh and aged emissions from new generation gasoline direct injector engines retrofitted with a gasoline particulate filter (GPF). Furthermore, ageing and subsequent secondary aerosol formation is explored in $(NH_4)_2SO_4$-seeded and non-seeded experiments. We explore the impacts on measured and predicted hygroscopicity, CCN-activity, and droplet kinetics of secondary aerosol mixed with initially insoluble carbonaceous materials versus very soluble $(NH_4)_2SO_4$ seed. The chemical composition and density of the secondary aerosol (SA) formed from aging is measured with an HR-TOF-AMS and a custom-built APM-SMPS system. The supersaturated and subsaturated hygroscopicity of the fresh and aged emission is measured with a DMT Streamwise Thermal Gradient CCN counter and a hygroscopicity tandem differential mobility analyzer (HTDMA), respectively.

The measurements show that the fresh gasoline emissions are only slightly hygroscopic in both supersaturated and subsaturated environments. Photochemical aging and subsequent condensation of the secondary aerosol formed from the co-emitted gas phase precursors increases the hygroscopicity of gasoline emissions. Without the GPF, both subsaturated and supersaturated hygroscopicity. When the engine was retrofitted with the GPF, the secondary aerosol (SA) experiments were seeded with $(NH_4)_2SO_4$. In these experiments the presence of the condensing SA depresses the hygroscopicity of the salt-secondary aerosol mixture. The hygroscopicity was also depressed in the subsaturated regime with time. These changes in the hygroscopicity with aging were additionally sensitive to aerosol dry size distribution. We also used threshold droplet growth analysis (TDGA) to evaluate the effects of the condensing SA on droplet kinetics.

These results have important implications for the assessment of cloud-aerosol indirect effects of salt-seeded and black carbonaceous aerosol cores. We concluded that in the new generation GDI vehicles the point of aerosol emissions will have significant influence on the impacts of the secondary and primary aerosols on climate.

## Introduction

Soot, formed from the incomplete combustion of fossil fuels, biofuel and biomass, forms a significant portion of the global aerosol budget; with an estimated 7600 Gg $yr^{-1}$ emitted in 2000 alone (Lamarque et al., 2010; Sasser et al., 2012). Soot is mainly composed of spherules of black carbon mixed with nitrates, sulfates and other organic and inorganic salts (Adachi & Buseck, 2008; Adachi et al., 2010). Soot particles have a net warming effect and when assumed to be internally mixed have warming effect second only to $CO_2$ (Ramanathan & Carmichael, 2008; Bond et al., 2013). Globally, about 20% of all black carbon emissions are from combustion related fossil fuel burning. The US Environmental Protection Agency (EPA) estimates more than 50% of black carbon emissions are from transportation sources (Sasser et al., 2012). Combustion soot, which vehicular soot makes up significant fraction of, may contribute up to 64% of the global CCN budget (Spracklen et al., 2011). It is therefore imperative to constrain the evolution and CCN potential of vehicular soot to improve our current estimation of anthropogenic direct and indirect forcing.

Fresh vehicular soot (combusted from various fuel sources) has exhibited no significant hygroscopic growth and CCN activity (Vu et al., 2017). The CCN concentration of combustion aerosol is mainly determined by the size distribution (Dusek et al., 2006), chemical composition (Jimenez et al., 2009) and morphology (Giordano et al., 2015). Tailpipe emissions are often assumed to be largely nucleation mode particles, mostly externally mixed, fractal composites with a significant insoluble volume fraction (Andreae & Rosenfeld, 2008). Little data exists on the aged CCN activity of complex vehicular emissions. *Tristcher et al (2011)* photochemically aged diesel soot and showed that secondary aerosol (mainly secondary organic aerosol and nitrates) formed form volatile organic carbon co-emitted with soot. Furthermore, the formation of secondary aerosol (SA) lead to changes in aerosol density, and increased both the sub-saturated (0.06 – 0.12) and supersaturated (0.09 – 0.14) hygroscopicity of the aerosol mixture. The hygroscopicity of aged diesel emissions was comparable to the hygroscopicity of chamber generated and ambient organic aerosol data sets (Chirico et al., 2010; Duplissy et al., 2011; Lance et al., 2013)

The secondary aerosol (SA) formed from both diesel and gasoline emission sources has been shown to be chemically similar (Presto et al., 2014). Thus the sub-saturated and supersaturated hygroscopicity and CCN activity of aged gasoline-generated soot are assumed to be similar to that of aged diesel, with kappa < 0.1 (Zaveri et al., 2010). To our knowledge, the subsaturated and supersaturated hygroscopicity of aged gasoline emissions has yet to be fully explored. Particularly, those from advanced gasoline engine technologies, (i.e., gasoline direct engines) that now dominate the gasoline vehicle market share.

During photochemical aging of vehicular emissions, the aerosol size distribution and morphology of the aerosol is significantly modified by the condensing SA. The condensation of the denser SA material increases the effective density of the aerosol and the volume equivalent diameter (Khalizov et al., 2013; Rissler et al., 2013; Giordano et al., 2016). Depending on the

miscibility, condensability, polarity and entropy, black carbon may form core shells, internal or external mixtures with the condensing SA and other atmospheric salts (nitrates, sulfates) (Asa-Awuku, Engelhart, et al., 2009; Vaden et al., 2010; Robinson et al., 2016). External mixtures are assumed to be weak non-homogenous conglomerates formed between the aerosol components. In internal mixtures, the aerosol components form a single-phase homogenous aerosol species. Black carbon is however solid and assumed immiscible and form multiphase core shell structures. External mixtures of BC and SA and salts are therefore more probable, especially after atmospheric transportation and aging (Jacobson, 2001; Moffet & Prather, 2009; Cappa et al., 2012).

Transportation emissions are a significant fraction of the total global PM emissions. One of the largest sources of vehicular emissions in the US is from light duty vehicles (LDV); passenger and trucks (Lamarque et al., 2010; Xing et al., 2013). With increasing LDV usage, the US Environmental Protection Agency (EPA) and the National Highway Transportation Safety Administration has promulgated legislation to increase the corporate average fuel economy(CAFE) and concurrently decrease the greenhouse gas emissions from LDV (Hula et al., 2015). The automobile industry responded to these new regulatory standards by developing and manufacturing more fuel efficient light duty vehicles. Improvements in fuel economy however modify emissions. For example, fuel efficient diesel vehicles incorporate diesel particulate filters to effectively remove enhanced soot emissions (EPA, 2012; Maricq et al., 2012).

Currently, gasoline direct injection (GDI) engines provide the best approach to meet both the new CAFE and GHG emissions standards (Yi et al., 2009; Hula et al., 2015; Ellies et al., 2016) . In GDI engines, the fuel and air is injected into the combustion chamber separately (Iwamoto et al., 1997; Zhang et al., 2012). This engine design provides higher power output, better fuel economy and fewer greenhouse gases. GDI engines however generate more particulate matter and number (PM/PN) as compared to equivalent port fuel injection engines. The reported higher PM and PN from GDI engines has been attributed to reduced time for inhomogeneous fuel air mixing, liquid gasoline impingement on the cylinder walls and piston resulting in regional fuel-rich combustion in the cylinder (Karavalakis et al., 2014; Wang et al., 2014). Efforts are therefore being made to integrate technologies and calibrate GDI engines to meet new, more stringent emissions standards. Proposals include modifications to the engine injector geometry and position to reduce fuel impingement, increasing fuel pressure and minimizing fuel droplet size, improve injection timing, engine downsizing and turbocharging and integrating gasoline particulate filters (GPF) (Yi et al., 2009; Piock et al., 2011; Whitaker et al., 2011).

Gasoline particulate filters (GPF) can remove up to 85% in applications with different gasoline blends over US EPA certified drive cycles (Chan et al., 2012; Chan et al., 2014). *Roth et al* (2017, in preparation) showed that the filtration of particulate black carbon by the GPF results in changes in the composition, morphology, density and size distribution of secondary aerosol mixtures formed from photochemical aging of the filtrate. With these changes in both physical

and chemical properties, it is important to constrain the corresponding subsaturated and supersaturated hygroscopicity, CCN activity and droplet kinetics of emissions from GDI vehicles with and without a GPF. This work complements the work of *Roth et al* (2017, in preparation) who during the same campaign characterized the secondary aerosol formation.

## Research Goals and Objectives

In this study, the first of its kind, we investigate:

1. The cloud condensation nuclei activity of freshly emitted and photochemically aged gasoline emissions from two light duty vehicles fitted with a GPF.
2. The CCN Potential from Low and High Mileage GDI vehicles
3. The impacts of organics, sulfates and nitrates fractional compositions on the CCN activity and hygroscopicity is also explored.

## Theory and Closure Analysis

### Supersaturated Hygroscopicity

Aerosol activate into cloud droplets and act as cloud condensation nuclei when exposed to a critical water vapor supersaturation, $s_c$. The critical supersaturation depends, mainly, on the aerosol dry size and chemical composition. Köhler theory incorporates the solute and curvature effects on equilibrium water vapor pressure. Köhler theory relates the thermodynamic and physical properties of aerosol to predict the critical supersaturation, $s_c$, at which an aerosol of dry size $D_d$, will activate into CCN (Köhler, 1936; Seinfeld & Pandis, 2006). Kohler theory can be defined as:

$$\ln S_c = \left(\frac{4A^3\rho_w M_s}{27v\rho_s M_w d_s^3}\right)^{\frac{1}{2}} \quad [1]$$

where,

$$A = \frac{4\sigma_{s/a} M_W}{RT\rho_w}$$

Where $S_c$ is the critical water-vapor saturation ratio for a dry-particle critical diameter $d_s$. The particle has a density $\rho_s$, a molecular weight $M_s$, and the Kelvin effect is represented by A. $M_w$ and $\rho_w$ are the molecular weight and density of water respectively and $v$ is the number of ions resulting from the dissociation of one solute molecule, $\sigma_{s/a}$ is the surface tension, $R$ is the universal gas constant and $T$ is the sample temperature. $S_c$, the critical saturation is greater than 1, the critical supersaturation $s_c$, is defined as $s_c = S_c - 1$.

In the absence of available solute and aerosol composition data, especially for ambient aerosol, Köhler theory is parameterized by a single hygroscopicity parameter, $\kappa$. The single parameter, $\kappa$

integrates aerosol compositional, size distribution and ambient water vapor concentration data. This enables an easy, robust representation of CCN activity in CCN models. Inorganic salts, such as ammonium sulfate and sodium chloride, which are generally highly hygroscopic, have a $\kappa$ between 0.5 and 1.2 whereas slightly hygroscopic to hygroscopic organic salts and secondary organic aerosol have a $\kappa$ between 0.01 and 0.5. Non-hygroscopic but wettable aerosol such as black carbon has a near zero $\kappa$ (Petters & Kreidenweis, 2007). The single parameter supersaturated CCN hygroscopicity, $\kappa_{CCN}$ can be defined by:

$$\kappa_{CCN} = \frac{4A^3}{27d_s^3 ln^2 S_c} \quad [2]$$

## Sub-saturated Hygroscopicity

The subsaturated water uptake by dry aerosol can be studied with the humidified tandem differential mobility analyzer (HTDMA) technique. An initial differential mobility analyzer (DMA) scans mono-dispersed, diffusion-dried aerosol, the aerosol distribution is then exposed to an elevated relative humidity (RH) in a conditioner where the particle takes up water. A second DMA is used to obtain a the humidified aerosol distribution and the ration between the peak dry distribution mobility diameter, $D_{in}$ and peak humidified aerosol distribution mobility diameter, $D_{RH}$ is the diameter growth factor (Schwarz et al.) which indicates the increase in the radial thickness of the aerosol (Rader & McMurry, 1986; Gysel et al., 2009).

HTDMA data can be fitted to obtain a single parameter hygroscopic factor similar to the fit for CCN data by fitting the GF as a function of RH (Petters & Kreidenweis, 2007; Kreidenweis & Asa-Awuku, 2014). Parameterization of HTDMA growth factor data with the single parameter $\kappa$ allows for the integration of HTDMA data into climate models. The single hygroscopic factor, $\kappa$ can be defined as:

$$\kappa_{HTDMA} = [GF^3 - 1]\left[\frac{100}{RH}\, exp\left(\frac{4\sigma_{s/a}M_w}{RT\rho_w D_{in}}\right) - 1\right] \quad [3]$$

If the Kelvin effects, the change in the water vapor pressure due to the curvature of the growing droplet, and $\kappa$ is assumed constant over a given RH range (valid for RH > 85%) (Khvorostyanov & Curry, 2007; Petters & Kreidenweis, 2007), then $\kappa_{HTDMA}$ can be estimated as follows:

$$\kappa_{HTDMA} = 0.111[(GF)^3 - 1] \quad [4]$$

## $\kappa$-hygroscopicity Closure

The assumptions used to estimate the simplified Köhler theory-based relationships for CCN activity information from sub-saturated and supersaturated instruments are extensive. CCN closure studies allows for the evaluation of these assumptions for suitability and robustness.

Several studies have sought closure between the $\kappa_{CCN}$ and $\kappa_{HTDMA}$ in ambient and laboratory-generated aerosol with varying degrees of discrepancy observed (Prenni et al., 2007; Alfarra et al., 2013; Whitehead et al., 2014; Zhao et al., 2016). The estimated subsaturated, $\kappa_{HTDMA}$ is almost always lower than the supersaturated, $\kappa_{CCN}$ . This may be attributed to surface tension, volatilization of organics, non-spherical dry aerosol and short residence times in the HTDMA (Massoli et al., 2010; Dusek et al., 2011; Frosch et al., 2011). Organic species may volatize between the first and second DMA and this may affect the initial dry aerosol size, $D_{in}$ (Prenni et al., 2001) . Non-spherical aerosol, prevalent in combustion, from the first DMA may collapse and restructure resulting in un-conserved aerosol dry volume and inaccurate growth factor prediction and $\kappa$ estimation (Mikhailov et al., 2009). The short residence time in subsaturated HTDMA may also limit aerosol dissolution, especially in coated aerosol and delay the equilibrium, thereby limiting the mass transfer of water vapor to the surface of the aerosol (Chan & Chan, 2007; Modini et al., 2010). Closure studies allow for the quantification of these factors on the hygroscopicity and CCN activity of the aerosol.

The focus of many supersaturated CCN closure studies compares ambient CCN activity with predictions by coupling compositional, size and CCN data from available fast resolution instrumentation. These studies are done to constrain the effects of aerosol mixing states, size dependent composition and droplet kinetics. The mixing state of aerosols has significant influences on the CCN activity and droplet concentrations (Cubison et al., 2008; Asa-Awuku et al., 2011). Assuming internal mixtures enables the use of bulk chemical composition properties but may result in an over-prediction of CCN concentrations and hygroscopicity (Lance et al., 2009; Wang et al., 2010). Incorporating hygroscopic and organic composition data can improve the agreement between the predicted CCN number and the hygroscopicity (Gunthe et al., 2009; Chang et al., 2010). CCN activity constrained with composition data (such as from an aerosol mass spectrometer) enables the evaluation of the influence of mixing states and bulk chemical composition assumptions on the estimated hygroscopicity and CCN activity.

# Experimental and Analytical Methods

## Setup and Instrumentation

The experiments were done at University of California, Riverside's Center for Environmental Research and Technology as part of a multi-agency funded study. The study evaluated tailpipe particulate matter emissions, secondary organic aerosol (SOA) formation and CCN activity of aged emissions from gasoline direct injection (GDI) light duty vehicles (LDV) prevalent in the California fleet. The secondary aerosol generation and characterization experiments from these specific vehicles are more elaborately described in Roth et al (2017, in preparation). Here, we only dwell on the aspects of the data and experimental setup that are pertinent to explaining CCN formation and hygroscopicity. The experimental setup of pertinent instruments and facilities is shown in Figure 1.

Two LDV wall-guided GDI vehicles, 2016 Ford Fusion and 2016 Mazda 3, were run on a Burke E. Porter light duty chassis dynamometer on the California Unified Cycle. The tailpipe emissions

were sampled via constant volume sampler and diluted. An AVL Micro soot sensor and a suite of other particle and gas measurement instrumentation was used to characterize the primary soot emissions. The soot was sampled directly from the dilution system into a portable mobile atmospheric reactor. In another setup, the vehicle's exhaust system was modified to include a gasoline particulate filter (GPF). The GPF can remove about 90% of the PM (Chan et al., 2012; Chan et al., 2014) In the GPF-fitted experiments, atomized aerosol $(NH_4)_2SO_4$ was injected into the reactor to serve as seeds (additional surface area) for secondary aerosol formation.

The primary emissions were aged in a 30 $m^3$ fluorinated ethylene propylene mobile film reactor. The primary tailpipe emissions; soot only or GPF-filtered soot + $(NH_4)_2SO_4$, is photo-oxidized for an average of 8 hours under ultra-violet lights and with hydrogen peroxide oxidant (70 – 140 µL) (Roth et al 2017, in preparation). The particulate mass, mainly SOA and nitrates, generated during photochemical oxidation are herein collectively referred to as secondary aerosol (SA). The SA formed during photooxidation experiments from the default engine after-treatment configuration without GPF, Mazda 3 and Ford Fusion experiments, are hereafter referred to as BCSA I and BCSA II, respectively. The secondary aerosol formed from the $(NH_4)_2SO_4$-seeded experiments are SSA I and SSA II, respectively. Each experimental iteration was done in triplicates; 12 unique experiments were performed. Results presented here are averages of at least two runs of one vehicle setup. The particle composition of the aerosol mixture was characterized by a high-resolution time-of-flight mass spectrometer (HR-TOF-AMS; Aerodyne Research Inc.) (Canagaratna et al., 2007). The aerosol effective density, $\rho_{eff}$, was measured with a customize-built aerosol particle mass analyzer (APM) –Scanning mobility particle sizer (SMPS) system. It has a 75s resolution. A custom LabVIEW® program actively optimized the instrument response by determining the peak diameter form two parallel SMPS to correct the mass of the particle estimated by the APM (Malloy et al., 2009).

The subsaturated hygroscopic growth of the BCSA and SSA is continuously measured with a custom-built HTDMA. Based on the Radar and McCurry design, the initial dry aerosol size distribution is measured by the first SMPS and then humidified (RH 85% - 95%) for about 1 min. A second SMPS measures the post-humidification size distribution. The ratio of the peaks of the lognormal size distributions is the GF (Rader & McMurry, 1986; Cocker et al., 2001; Qi et al., 2010). The CCN activity was measured with a DMT Inc. CCN counter (CCNc) coupled with a TSI Inc. SMPS system. The size distribution from the SMPS (10 – 500 nm) operating in scanning mode, is exposed to scanning superstation (0.8 - 1.8%) in the CCN counter (CCNc) at a sample flowrate of 0.5 lpm. The CCN counter provides CCN concentration and droplet size information at 1Hz resolution. This is inverted with the SMPS dry size data to infer the CCN activity and hygroscopicity. The CCNc flowrates and supersaturation was calibrated within 10% of the flowrate and supersaturation set points before the experiments with laboratory-generated $(NH_4)_2SO_4$ (Lance et al., 2006; Rose et al., 2008).

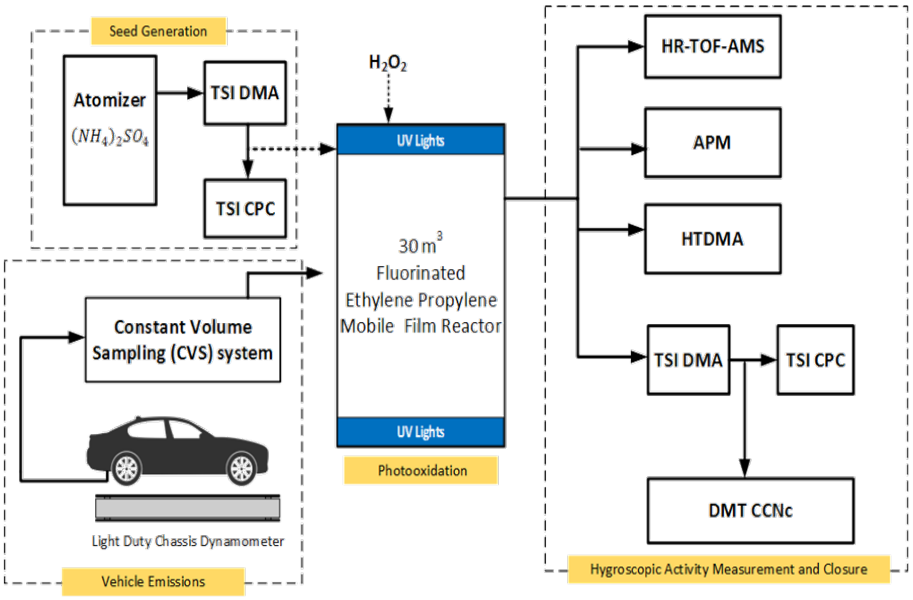


**Figure 1. Experimental setup for Tailpipe emissions measurement, SA generation and hygroscopicity measurement**

## Determining *κ*-hygroscopicity

An apparent CCN hygroscopicity parameter, $\kappa_{CCN}$ was measured from the CCN counter and SMPS data with scanning mobility CCN analysis, SMCA (Moore et al., 2010). The dry aerosol number, CN is derived from inverting the aerosol time series data from the SMPS. Multiple charge-corrected dry size distribution and CCN time series are synchronized to estimate an activation ratio (CCN/CN). The critical diameter, $dp_{50}$, is the diameter at which more than half of the aerosol dry size distribution activates at a specific supersaturation, $s_c$ (Moore et al., 2010). The $dp_{50}$ is equivalent to $D_d$ in equation [4.2]. In using equation [4.2] to estimate $\kappa_{CCN}$, we assumed SSA and BCSA were internally mixed or formed core-shell structures, respectively.

Equation [4.3] is employed to estimate the subsaturated HTDMA hygroscopicity parameter, $\kappa_{HTDMA}$. Only positive hygroscopicity values are reported. Negative $\kappa_{HTDMA}$ are not shown and indicate shrinkage in the aerosol size; as a likely a result of restructuring when exposed to the higher RH environment (Mikhailov et al., 2009; Ma et al., 2013). In calculating the $\kappa_{CCN}$ and $\kappa_{HTDMA}$, the surface tension of pure water in the growing droplet was constrained with the instrument water vapor temperature (Pruppacher & Klett, 1997).

From *Petters et al (2007)*, the average volume-weighted *κ* of a mixture can be calculated from the individual volume fractions of the constituent species:

$$\kappa = \sum_i \varepsilon_i \kappa_i \qquad [5]$$

Where $\varepsilon_i$ is the volume fraction of component $i^{th}$ of the aerosol mixture.

Inorganic nitrate measured by the AMS was assumed ammonium nitrate with $\kappa$ of 0.75. The sulfates from the salt seeded experiments were assumed to be ammonium sulfate with a $\kappa$ of 0.6 and $\kappa$ of 0.15 was used for the organic fraction in line with chamber generated SOA (Petters & Kreidenweis, 2007; Suda et al., 2012). The total aerosol mass was assumed to be composed of refractory and non-refractory aerosol. Thus, the total mass is estimated from the initial black carbon mass (measured before photooxidation from the AVL micro soot sensor) and the secondary aerosol mass measured by the AMS. The total aerosol volume is estimated from this mass and the effective density, $\rho_{eff}$ from the APM-SMPS system. The residual volume after accounting for the AMS organics and inorganics is considered the volume of the black carbon component. An average hygroscopicity, $\kappa_{BC}$ of 0.001 was applied to freshly emitted soot (Zaveri et al., 2010; Vu et al., 2015). Assuming simple mixing (Petters & Kreidenweis, 2007), the average hygroscopicity based on the aerosol mass fractions as follows:

$$\kappa_{AMS} = \varepsilon_{inorg}.\kappa_{inorg} + \varepsilon_{org}.\kappa_{org} + \kappa_{BC}.(1 - \varepsilon_{inorg} + \varepsilon_{org}) \quad [6]$$

Where *inorg* and *org* are the inorganic and organic property values respectively.

## Determining Droplet Kinetics

The droplet growth and kinetics effects of the condensing SA on either the BC or $(NH_4)_2SO_4$ is evaluated through threshold growth analysis (TDGA) (Engelhart et al., 2008; Asa-Awuku, Engelhart, et al., 2009). TGDA detects the presence of slowly activating components during the evolution of both SSA and BCSA. This method has been applied to various ambient and laboratory-generated aerosol to varying effect. In TDGA the average droplet diameter of activated CCN exiting the CCN counter optical particle counter (OPC) is compared to a standard aerosol with rapid activation kinetics at the same supersaturation $S_c$ and instrument settings. In this study laboratory-generated $(NH_4)_2SO_4$ aerosol is used as the reference. Absent mass transfer limitations, slow activating and surface active fractions and depletion effects, the reference aerosol and the BCSA and SSA should all grow to similar droplet sizes (Padró et al., 2010; Asa-Awuku et al., 2011; Engelhart et al., 2011; Ruehl et al., 2016; Fofie, Castellucio, et al., 2017). The reported droplet diameters are corrected for droplet size depletion by the CCN number (Lathem & Nenes, 2011). It should also be noted that the optical particle counter on the CCNc has a bin width of 0.5 µm hence any droplet size differences less than 1 µm are not be robustly differentiated (Fofie, Castellucio, et al., 2017).

# Results

## Supersaturated Hygroscopicity

The supersaturated $\kappa_{CCN}$ was estimated using the methods and assumptions described in section 3.2 and equation [4.2]. The average apparent $\kappa_{CCN}$ for the BCSA mixtures over the entire experiment, after the UV lights were turned on, was $0.11 \pm 0.07$. This is within the range of previously reported CCN hygroscopicity for laboratory-aged combustion soot (Zaveri et al., 2010; Tritscher et al., 2011). Whiles the average SSA $\kappa_{CCN}$ before the UV lights were turned on was $0.50 \pm 0.07$ and $0.42 \pm 0.09$ after the UV lights are turned on. This is also consistent with previously documented hygroscopicities of SOA coated salt mixtures from chamber experiments (Huff Hartz et al., 2005; King et al., 2009; Shantz et al., 2010).

In Figure 2, we observe changes in the hygroscopicity as a function of time and dry diameter. In the BCSA I and BCSA II experiments (Figures 2a and 2b), the first 30 minutes show hygroscopicities similar to unaged vehicle soot, $\kappa_{CCN} = 0.0014 \pm 0.0006$ (Tritscher et al., 2011; Vu et al., 2017). As the emissions age, however, the SA formed from the co-emitted gas phase precursors condense onto the BC core (Roth 2017, in preparation) and increase the hygroscopicity. In the BCSA II experiments, the CCN hygroscopicity increases to levels above that of average SOA (peak $\kappa_{CCN} = 0.3$) indicating the formation of species more hygroscopic than slightly soluble organics. *Roth et al (2017*) shows the formation of elevated amounts of nitrates may account for the sudden spike in hygroscopicity. In BCSA I there is a gradual increase in the hygroscopicity during the course of the experiment but the maximum $\kappa_{CCN}$ ($\kappa_{CCN} = 0.125$) remains below that of SA indicating the dominance of the black carbon component on the hygroscopicity. In the SSA experiments (Figures 2c and 2d), the hygroscopicity is significantly dominated by the ammonium sulfate seeds.

The formation of SA however, does significantly suppress the average $\kappa_{CCN}$, reducing it from 0.55 to 0.42. This suggests an internally mixed aerosol of ammonium sulfate, BC and SA as consistent with previous ambient and experimental observations (Wang et al., 2010).

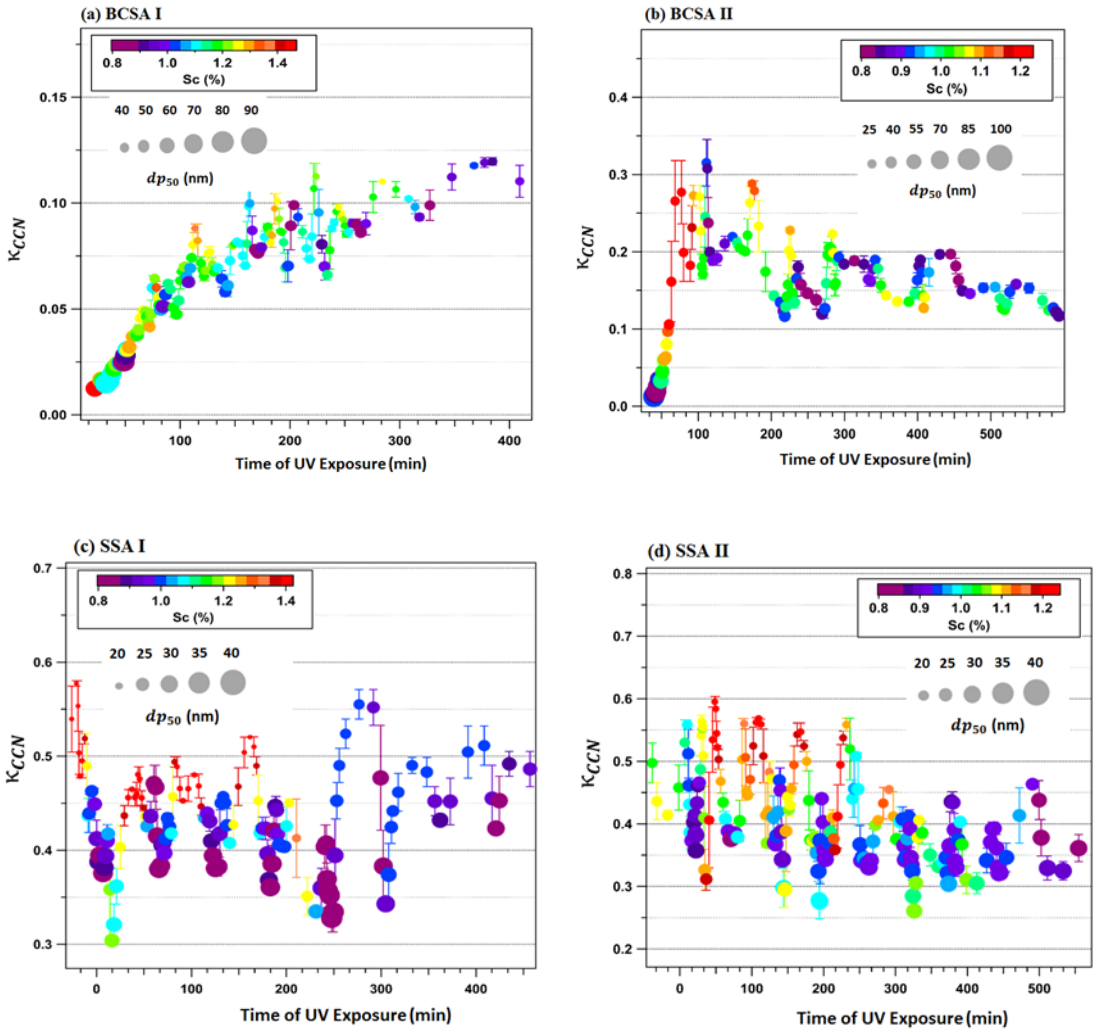


**Figure 2. Evolution of the CCN hygroscopicity, $\kappa_{CCN}$ with experimental time. The UV lights are turned on at time = 0 minutes.**

There is a sensitivity of the hygroscopicity to the critical dry diameter, $dp_{50}$ . In the SSA systems, irrespective of the experimental elapsed time, the larger dry aerosol ( $dp_{50} = 40\ nm$) were the least hygroscopic ($\kappa_{CCN} = 0.3$) and more hygroscopic ($\kappa_{CCN} = 0.5$) at the smaller critical diameters ($dp_{50} = 20\ nm$). This suggests that at the smaller dry SSA sizes the more soluble, hygroscopic $(NH_4)_2SO_4$ volume faction dominates the CCN activity. In the BCSA system, the hygroscopicity is relatively insensitive at $dp_{50} \gg 60\ nm$. The more hygroscopic nitrates and organics have a higher propensity to condense onto the smaller size BC particles. The resultant BCSA are less fractal with a greater CCN active surface area, thus the apparent supersaturated hygroscopicity increases (Figures 2a and 2b).

## Sub-saturated Hygroscopicity

The sub-saturated hygroscopicity, $\kappa_{HTDMA}$ was calculated from the HTDMA data using equation [4.4]. The HTDMA was operated at $RH = 0.93 \pm 0.04$. The BCSA particles had a $GF = 1.06 \pm 0.02$ and $\kappa_{HTDMA} = 0.006 \pm 0.005$ before the UV lights were turned on. The GF reduced to $1.007 \pm 0.005$ with $\kappa_{HTDMA} = 0.015 \pm 0.036$ after the lights were turned on. In the SSA the average GF before the UV lights were turned on was $1.31 \pm 0.21$ and $\kappa_{HTDMA} = 0.18 \pm 0.04$ with a reduced growth factor of $1.26 \pm 0.17$ and $\kappa_{HTDMA} = 0.10 \pm 0.14$ after the lights were turned on. The $\kappa_{HTDMA}$ was evaluated for aerosol dry sizes, $D_{in}$, from 60 to 260 nm initially selected by the first DMA.

In Figure 3, we observe changes in the subsaturated hygroscopicity, $\kappa_{HTDMA}$ during the evolution of the emissions. In the BCSA I and II (Figures 3a and 3b) aerosol is initially very non-hygroscopic ($\kappa_{HTDMA} = 0.002 \pm 0.0007$ for BCSA I and $\kappa_{HTDMA} = 0.0003 \pm 0.007$ for BCSA II).The formation and condensation of SA from the co-emitted gas phase components onto the BC core increases the $\kappa_{HTDMA}$. The variation in $\kappa_{HTDMA}$ is highly sensitive to the peak of the dry aerosol distribution, $D_{in}$ selected by the first DMA. In the BCSA I, the $\kappa_{HTDMA}$ increases to as much as $0.11 \pm 0.03$ after 500 minutes of photochemical oxidation at an average peak dry diameter, $D_{in}$of 120 nm. In the BCSA II however, after 600 minutes of photochemical oxidation the $\kappa_{HTDMA}$ increases to $0.03 \pm 0.0074$ at an average peak dry diameter of 260 nm. In the SSA however, there was an observed depression in the measured $\kappa_{HTDMA}$ with increase in the peak dry size. In the SSA I mixture the low hygroscopicity ($\kappa_{HTDMA} = 0.024 \pm 0.001$ ) was observed for the large dry sizes of 225 nm whiles the mixture is most hygroscopic ($\kappa_{HTDMA} = 0.19 \pm 0.02$) at an average dry size of 115nm before the UV lights were turned on.

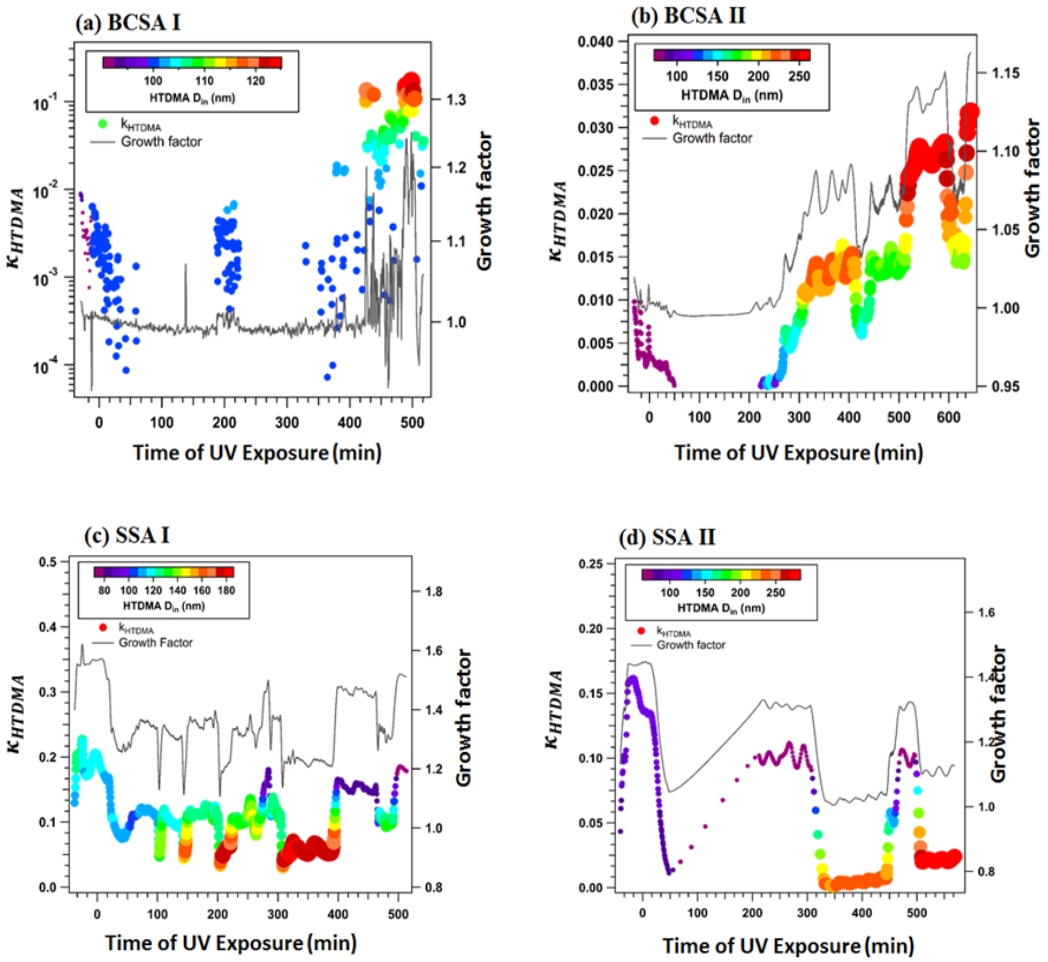


**Figure 3. Evolution of the HTDMA hygroscopicity, $\kappa_{HTDMA}$ with experimental time. The UV lights are turned on at Time = 0 minutes. Only positive $\kappa_{HTDMA}$ values are shown.**

We observe similar trends in the secondary aerosol formed from the 2nd vehicle (SSA II). The SSA II mixture is the least hygroscopic ($\kappa_{HTDMA} = 0.021 \pm 0.002$) at a peak average dry size of 280nm. SSAII was the most hygroscopic ( $\kappa_{HTDMA} = 0.15 \pm 0.02$ ) at an average dry size of 100nm before the UV lights were turned on. The higher hygroscopicity observed in the SSA before the lights were turned on is consistent with the presence of greater volume fractions of more soluble $(NH_4)_2SO_4$. The formation and condensation of SA onto the salt core depresses the solubility and hygroscopicity of SSA. The lowest $\kappa_{HTDMA}$ in the SSA is equivalent to the largest hygroscopicity in the BCSA confirming the more soluble secondary material is the main driver of hygroscopicity in the subsaturated regime. The quantitative contributions of the secondary aerosol to supersaturated and subsaturated particle hygroscopicity are evaluated with a closure study in subsequent sections.

## Droplet Kinetics

In Figure 4, the droplet sizes of the mixtures is compared to the droplet sizes of laboratory-generated $(NH_4)_2SO_4$ aerosol. The droplets are evaluated at 0.5 lpm CCNc flowrate and 0.8 – 1.6% supersaturation. The droplets sizes are corrected for depressions due to the CCN concentrations (Lathem & Nenes, 2011; Fofie, Castellucio, et al., 2017).

In Figure 4a, the condensation of the SA onto the BCSA does not seem to modify the droplet kinetics. The average final droplet diameters of BCSA, for all supersaturations evaluated, was within $\pm 4\%$ of the $(NH_4)_2SO_4$ reference diameters. Changes in the volume fraction of the secondary aerosol ($NO_3$ + organics) does not significantly modify the droplet sizes. These results suggest that the integration of BC into the SA to form core shell structures does not substantially modify the kinetics of the SA. In Figure 4b, there is a more significant modification of the SSA droplet kinetics. The average final droplet diameters for SSA, for all supersaturations evaluated, were an average of one bin size and up to 7% smaller than the $(NH_4)_2SO_4$ reference diameters (Fofie, Castellucio, et al., 2017). This suggests that the integration of the $(NH_4)_2SO_4$ and SA into internal mixtures results in relatively slower droplet kinetics.

These results are in agreement with previously reported droplet kinetics from chamber SOA (Engelhart et al., 2008; Zhao et al., 2016) and ambient data sets (Bougiatioti et al., 2009). Contrary to previous observations in ambient aerosol, the presence of the insoluble BC fraction does not seem to significantly retard the droplet growth kinetics in BCSA (Padró et al., 2010; Asa-Awuku et al., 2011). The modifications in droplet kinetics in SSA may not be statistically insignificant since they are within one bin width (0.5 µm) of the optical particle counter (Fofie, Castellucio, et al., 2017).

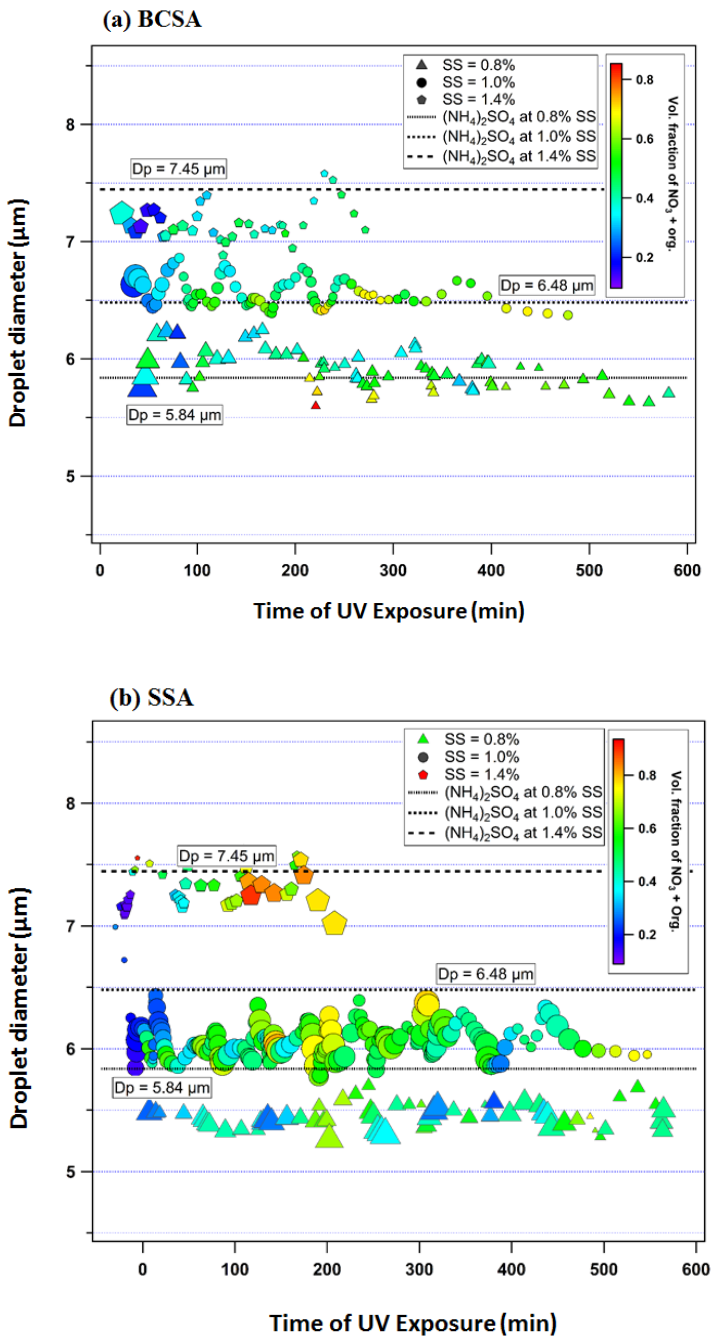


**Figure 4. The droplet diameters of (a) BCSA and (b) SSA compared to that of $(NH_4)_2SO_4$. Each point is the mean droplet diameter at the specified supersaturation over the course of the experiment.**

# Closure Analysis

## Closure between CCN Measured and AMS Derived κ-Hygroscopicity

The $\kappa$-hygroscopicity parameter measured from the CCN experiments is compared to hygroscopicity,$\kappa_{AMS}$ values calculated from HR-TOF-AMS and APM data using equation [6]. In Figure 5, by comparing the slopes, *S* of the fits, there is an observed general convergence of the bulk $\kappa$-hygroscopicities, $\kappa_{AMS}$ and $\kappa_{CCN}$ for all systems (S= $1.005\ to\ S = 1.13$) except in BCSA II ($S = 1.91$) (Figure 5b).

The influence of the dry aerosol size on the CCN analysis seems to be minimal in both BCSA and SSA. The aerosol shows a uniform, size-independent chemical composition (except in BCSA II). The higher dry aerosol detection limit of the AMS does not therefore seem to adversely bias the closure. The convergence in the mobility diameter derived $\kappa_{CCN}$ and the mass fraction based $\kappa_{AMS}$ hygroscopicities indicates that the bulk composition assumptions inherent in CCN SMCA analysis are sound for this aerosol system. Constraining the aerosol volume with the effective density, $\rho_{eff}$ data from the APM-SMPS system ensured a robust prediction of the aerosol volume. $\rho_{eff}$ accounts for the mixture morphology and fractal nature as SA condenses onto the core (DeCarlo et al., 2004; Nakao et al., 2011; Giordano et al., 2015).

The non-closure observed in BCSA II may be due to a non-uniform, size dependent chemical composition of the aerosol mixture. *Roth et al* (2017) observed a nucleation burst after 100 min accompanied by a significant formation of nitrates. The nitrate-rich nucleation formed mainly larger dry aerosol beyond the scope of CCN measurements. The BCSA II $\kappa_{AMS}$ is size-dependent and is driven by the higher nitrate volume fraction, hence the non-convergence observed.

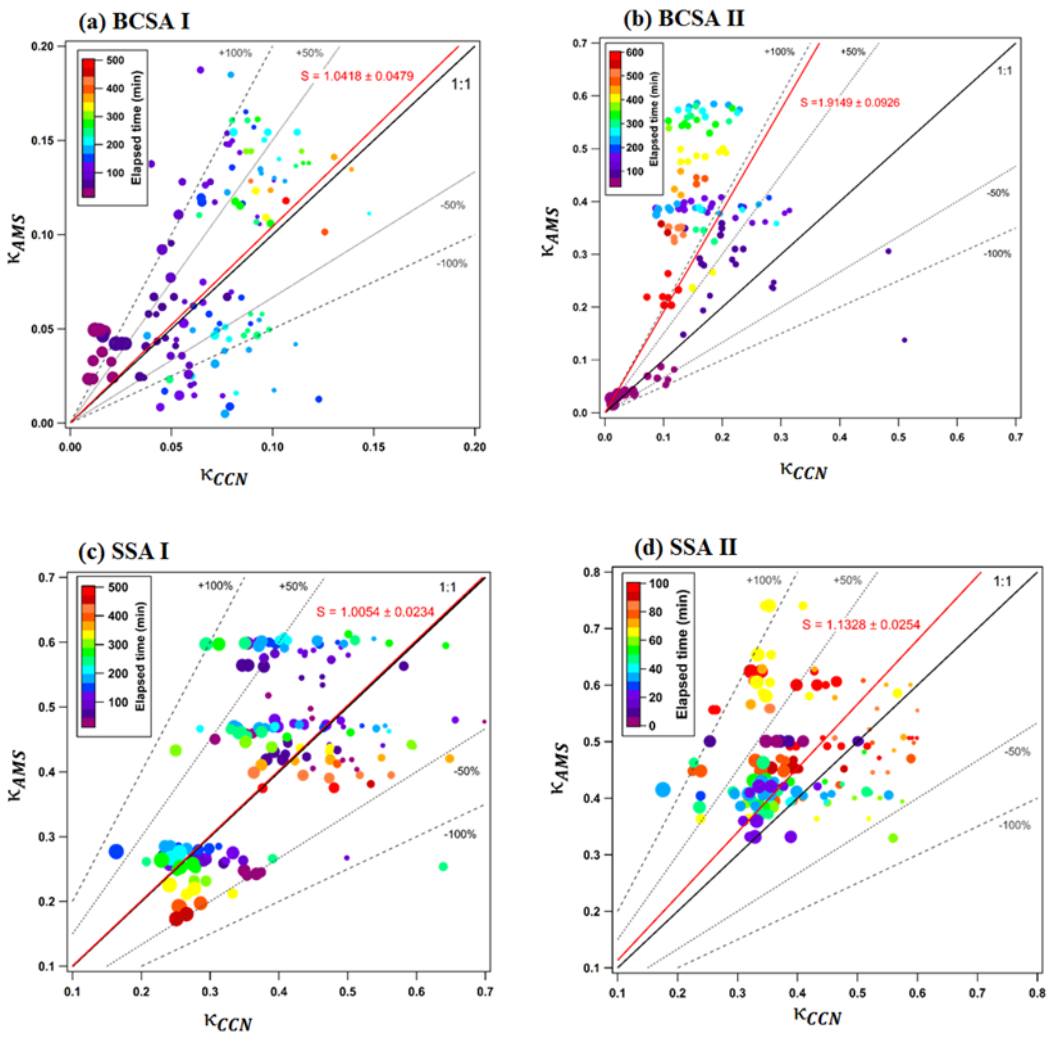


**Figure 5. Closure analysis of CCN hygroscopicity with AMS data. Solid red line represents the slope, *S* of the fit. Dashed lines represent $\pm 50\%$ and $\pm 100\%$ prediction error.**

## Closure between CCN and HTDMA κ-hygroscopicity

The $\kappa$-hygroscopicity parameter computed from the supersaturated CCNc and the subsaturated HTDMA is compared to evaluate the convergence of the two approaches in Figure 6. There is significant difference between the $\kappa_{HTDMA}$ and $\kappa_{CCN}$. The $\kappa_{HTDMA}$ was lower than $\kappa_{CCN}$ in both systems. The ratio of $\kappa_{HTDMA}/\kappa_{CCN}$ in BCSA I and BCSA II is 0.10 and 0.42, respectively. The of $\kappa_{HTDMA}/\kappa_{CCN}$ for SSA is 0.27 and 0.13, respectively. There is therefore a larger difference between the hygroscopicities in the SSA than in BCSA. The non-closure observed in the measured sub- and super-saturated can be attributed to various factors including solubility, nonsphericity, non-conservation of morphology, and volatilization of volatile organic components (Prenni et al., 2007; Petters et al., 2009; Massoli et al., 2010; Alfarra et al., 2013).

The solubility of the aerosol has a significant effect on both the subsaturated and supersaturated hygroscopicity. The solubility effects have however been observed to be more noticeable in the subsaturated HTDMA measurement. (Petters & Kreidenweis, 2008). The SSA $\kappa_{HTDMA}$ although higher than that of BCSA is not equivalent to that of $\kappa_{CCN}$. The presence of the condensed, less soluble SOA fraction on the BC and $(NH_4)_2SO_4$ may suppress the influence of the more soluble $(NH_4)_2SO_4$ on $\kappa_{HTDMA}$. Less soluble aerosol requires higher relative humidity to activate into the droplets. The higher supersaturations (0.8 - 1.6%) at which the CCN was operated activated smaller aerosol into droplets as compared to the HTDMA (~ RH = 94%). The $\kappa_{CCN}$ is based on bulk average chemical composition hence the effects of the non-uniform, size dependent chemical composition on hygroscopicity, as suggested by $\kappa_{HTDMA}$, are absent. The lower solubility coupled with a lower residence time and larger sizes in the HTDMA results in the lower measured hygroscopicities in both BCSA and SSA.

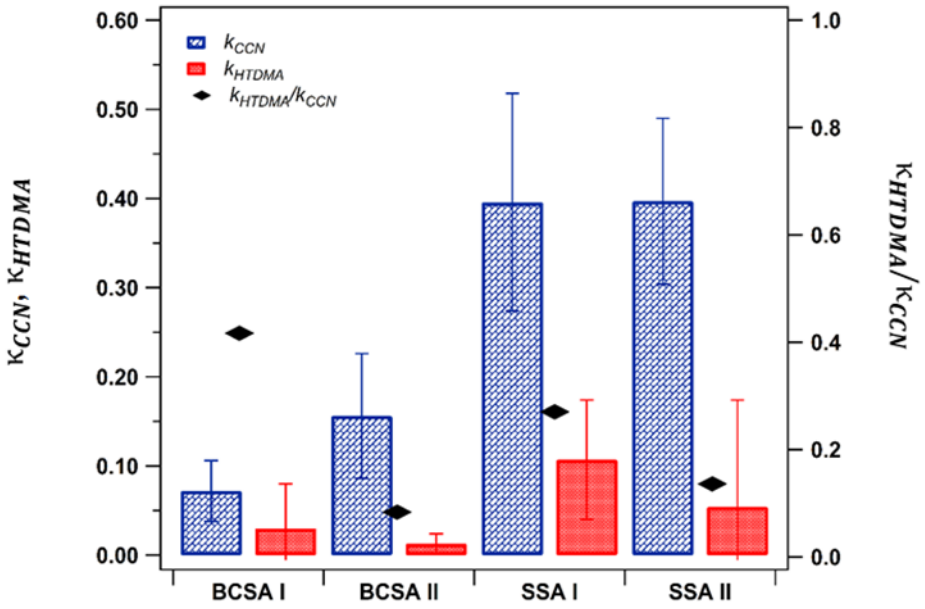


**Figure 6. Comparison between $\kappa_{CCN}$ and $\kappa_{HTDMA}$ .**

## Effects of the Aerosol Volume Fraction on CCN hygroscopicity

In aerosol mixtures, the hygroscopicity has been shown to be volume additive and solubility influenced. This is well characterized in known, simple aerosol mixtures of salts and organic aerosol (Riipinen et al., 2015). In photochemically aged combustion aerosol and SOA however, the more complex chemical composition and mixing states makes constraining the hygroscopicity with the volume fractions challenging (Asa-Awuku, Miracolo, et al., 2009; Fofie, Donahue, et al., 2017).

In Figure 7, the complex aerosol mixtures formed are constrained by the component volume fractions. In Figure 7a, the organic aerosol fraction in BCSA remains relatively unchanged. The bulk of the secondary aerosol volume is from the nitrates.

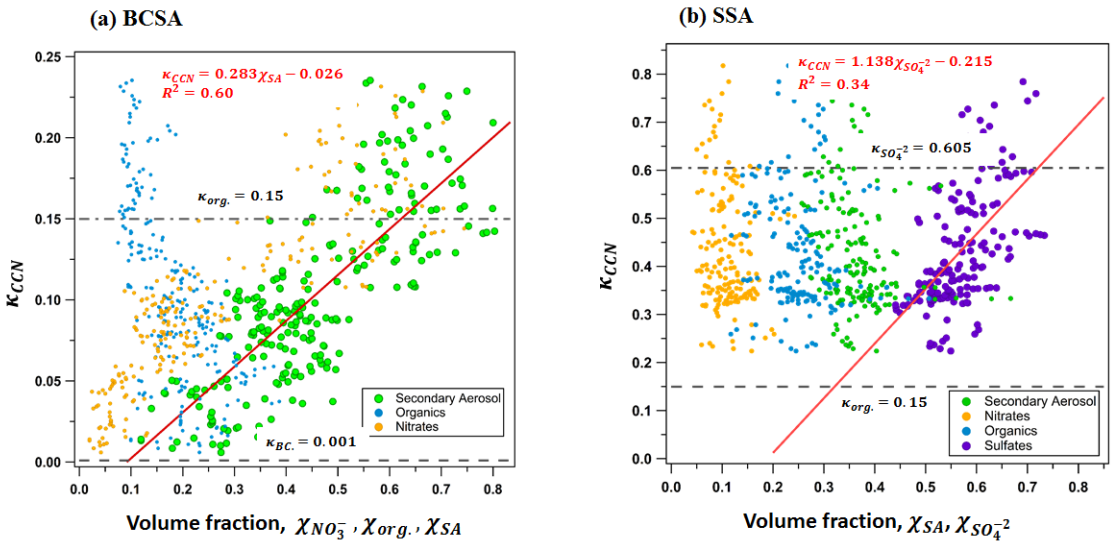


**Figure 7. Effects of the aerosol volume fractions on the $\kappa_{CCN}$ . Solid red line is the linear fit.**

The BC fraction limits the supersaturated hygroscopicity, $\kappa_{CCN}$ of the mixture when the secondary aerosol volume fraction $\chi_{SA} < 0.1$ of the total aerosol volume. Thereafter, the hygroscopicity increases linearly with increasing SA volume fraction ($\kappa_{CCN} = 0283_{\chi_{SA}} - 0.026, R^2 = 0.60$). When $\chi_{SA} = 0.6$, the $\kappa_{CCN}$ is equivalent to that of secondary organic aerosol ($\kappa_{SOA} = 0.15$) although more than 0.4 of the $\chi_{SA}$ fraction is from the more soluble, hygroscopic nitrates. In Figure 7b, the sampled SSA aerosol showed unchanged SA volume fractions. The $(NH_4)_2SO_4$ fraction reduced with increasing formation and condensation of SA. The formation of nearly equi-volume fractions of the components suggest homogenous, internally mixed aerosol. The hygroscopicity is higher than $\kappa_{SOA}$ and $\kappa_{(NH_4)_2SO_4}$ but shows no distinct correlation between one fraction and hygroscopicity.

## Summary and Implications

In this study we investigated the hygroscopicity and droplet kinetics of secondary aerosol (BCSA and SSA) formed from emissions of light-duty vehicles with new engine technology. BCSA was formed from the photo-oxidation of the whole soot wiles SSA was formed from GPF-filtered, $(NH_4)_2SO_4$ – seeded soot. The sub- and super-saturated hygroscopic activity is characterized with HTDMA and CCN counter respectively. The aerosol chemical composition, mixing states and morphology are constrained with information an AMS and APM-SMPS system. We found that aged soot from light duty vehicles are hygroscopic in supersaturated and subsaturated environments.

In supersaturated CCNc experiments, BCSA and SSA showed significant increase in hygroscopicity with photochemical aging ($\kappa_{CCN}$ = 0.001 – 0.32 in BCSA and $\kappa_{CCN} = 0.55 - 0.25$ in SSA). In the BCSA, condensation of nitrates onto the BC core is driving the hygroscopicity. The CCN activity in BCSA increases incrementally with the formation of SA. *Tritscher et al* (2011) recently observed similar trends in hygroscopicity in aged diesel soot. The condensation of the SA fills the void in the non-spherical freshly emitted soot (Nakao et al., 2011), the BC fractions however limits the $\kappa_{CCN}$ to levels less than the SA alone. This suggests a core-shell mixture with the SOA condensing onto a BC core (Wittbom et al., 2014). In BCSA I, with relatively lower mass of SOA forming, the black carbon component drives the hygroscopicity. There is a strong closure between $\kappa_{CCN}$ and $\kappa_{AMS}$ ($S = 1.0418 \pm 0.0479$). In BCSA II however, there is weak closure between the $\kappa_{CCN}$ and $\kappa_{AMS}$ ($S = 1.9149 \pm 0.0926$). The formation of high amounts of organics and nitrates modified the effective density ($\rho_{eff} = 0.66 - 1.87$) and morphology of BCSA II significantly (King et al., 2009). This results in an over-estimated electrical mobility diameter, $dp_{50}$ and under-prediction in $\kappa_{CCN}$. This core-shell assumption is buttressed by the sensitivity of $\kappa_{CCN}$ to larger aerosol dry sizes which have a higher nitrate fraction in BCSA II.

In SSA, the presence of the more hygroscopic $(NH_4)_2SO_4$ core drives $\kappa_{CCN}$ to levels higher than the SA. The continual condensation of SA onto the salt core depresses the hygroscopicity. The decrease in $\kappa_{CCN}$ with SA formation, but not to levels equal to SA alone, indicates the likely formation of an internal mixture of SA + $(NH_4)_2SO_4$ as observed and inferred in previous ambient and laboratory data sets (Riemer et al., 2004; Adachi & Buseck, 2008). The internal mixture hypothesis is confirmed by the robust closure between the $\kappa_{CCN}$ and the AMS-derived $\kappa_{AMS}$ (SSA I $S = 1.0054 \pm 0.0234$, SSA II $S = 1.1328 \pm 0.0254$) which assumes the aerosol is internally mixed and homogenous bulk properties. Similar trends in hygroscopic behavior has been observed in laboratory studies of salt-seeded SOA experiments (Engelhart et al., 2008; King et al., 2009) and speciated ambient aerosol (Bougiatioti et al., 2009; Dusek et al., 2010; Pöschl et al., 2010; Asa-Awuku et al., 2011). In both ambient and laboratory studies, the presence of SA caused a decrease in the hygroscopicity and CCN activity. This is likely attributed to depressions in the droplet surface tension, and to a lesser extent changes in morphology (density) and molar volume (King et al., 2009; Asa-Awuku et al., 2010; Ruehl et al., 2012).

In the sub-saturated HDTMA experiments, we observed similar dependence of the hygroscopicity, $\kappa_{HTDMA}$ on the seed type and SA condensation. The SSA mixtures showed higher hygroscopicity than BCSA. Although there was a modification in $\kappa_{HTDMA}$ with aging, the biggest driver of the hygroscopicity in the sub-saturated regime appears to be aerosol dry size. In BCSA, $\kappa_{HTDMA}$ increased with experimental evolution and increasing peak diameter. The solubility of BCSA is minimal in HTDMA (with short residence time and low RH) (Chan & Chan, 2005). The hygroscopicity is therefore constrained by the relatively more soluble SA fraction. In SSA the condensing SA is less soluble than the $(NH_4)_2SO_4$ seed, the $\kappa_{HTDMA}$ is therefore depressed at higher dry aerosol sizes which have higher SA volume fractions. This susceptibility of sub-saturated hygroscopicity in salt and SOA mixtures to volume fractions and dry size has previously been reported in ambient and laboratory data sets. Mixtures of $(NH_4)_2SO_4$ and SOA in chamber studies showed a decrease in hygroscopicity based on the volume fraction of the SOA

and the level of oxidation similar to our observations (Smith et al., 2012). The hygroscopicity has also been shown to be dependent on aerosol dry size, especially in multicomponent systems (Laskina et al., 2015). The weak closure observed between the $\kappa_{HTDMA}$ and $\kappa_{CCN}$ supports these assertions. Absent the solubility influences, a stronger convergence between $\kappa_{HTDMA}$ and $\kappa_{CCN}$ is expected especially in more soluble, $(NH_4)_2SO_4$ –seeded SSA. We however observe similar $\kappa_{HTDMA}/\kappa_{CCN}$ for BCSA (0.10 – 0.42) and SSA (0.13 - 0.27) indicating a higher dependence of the sub-saturated hygroscopicity on the condensing SA fraction than on the seed.

In terms of the droplet kinetics, we do not observe a significant modification due to either the condensing gases or seed. The TDGA analysis shows comparable final droplet diameters between BCSA, SSA and $(NH_4)_2SO_4$. The presence of the insoluble, un-wettable BC, even that which is internally mixed, does not modify the droplet growth significantly. This suggests that, post-activation, the solubility of the aerosol does not have a significant influence on the condensational growth of the droplet. The presence of the organics and sulfates do not also modify the droplet kinetics significantly, unlike in previously reported ambient CCN measurements of aged urban combustion aerosol (Asa-Awuku, Engelhart, et al., 2009; Asa-Awuku et al., 2011). The SA formed does however seem to modify the surface activity of the aerosol mixture in the $(NH_4)_2SO_4$-seeded SSA particles. The presence of surface-active, surface tension depressing organic components would have modified the mass transfer of water (characterized by the mass accommodation coefficient) and hence the smaller final droplet sizes (Ruehl et al., 2008; Ruehl et al., 2012; Noziere, 2016; Ruehl et al., 2016). The absence of distinguishable differences in droplet kinetics does not however conclusively indicate similar droplet kinetics considering the high supersaturation of the CCN (Engelhart et al., 2008) and the bin width of the CCNc optical particle counter (Fofie, Castellucio, et al., 2017).

The results from this study suggests that emissions from newer technology GDI engines form CCN active SA upon photochemical aging. The integration of gasoline particulate filters (which removes up to 90% of BC) will modify the hygroscopicity and CCN activity of the emissions based on the point of dispersion. In supersaturated urban environments where BC is abundant, the SA formed from GPF fitted GDI vehicles are more likely to condense onto BC and increase the hygroscopicity. In supersaturated rural regions, the SA will form mixtures (internal or external) with salts (nitrates, sulfates) and reduce the hygroscopicity of the new particle. In BC-core-shell mixtures, our results suggest that the hygroscopicity may be significantly inhibited by the less hygroscopic volume fraction. When the BC is removed however, hygroscopicity of the resulting internal mixtures are largely dependent on the most soluble, hygroscopic fraction (such as the cases where sulfates are dominant). It is therefore important to constrain the available seed chemical composition when modelling the effects of anthropogenic combustion vehicle emissions on cloud indirect effects. In the subsaturated environments however, the delinquency is only influenced by the SA coating making the point of emission dispersion unimportant to modeling cloud indirect effects.

## References


Adachi, K., & Buseck, P. R. (2008). Internally mixed soot, sulfates, and organic matter in aerosol particles from Mexico City. *Atmospheric Chemistry and Physics, 8*(21), 6469-6481. doi:10.5194/acp-8-6469-2008

Adachi, K., Chung, S. H., & Buseck, P. R. (2010). Shapes of soot aerosol particles and implications for their effects on climate. *Journal of Geophysical Research-Atmospheres, 115*(D15). doi:Artn D1520610.1029/2009jd012868

Alfarra, M. R., Good, N., Wyche, K. P., Hamilton, J. E., Monks, P. S., Lewis, A. C., & McFiggans, G. (2013). Water uptake is independent of the inferred composition of secondary aerosols derived from multiple biogenic VOCs. *Atmospheric Chemistry and Physics, 13*(23), 11769-11789. doi:10.5194/acp-13-11769-2013

Andreae, M. O., & Rosenfeld, D. (2008). Aerosol-cloud-precipitation interactions. Part 1. The nature and sources of cloud-active aerosols. *Earth-Science Reviews, 89*(1-2), 13-41. doi:10.1016/j.earscirev.2008.03.001

Asa-Awuku, A., Engelhart, G. J., Lee, B. H., Pandis, S. N., & Nenes, A. (2009). Relating CCN activity, volatility, and droplet growth kinetics of beta-caryophyllene secondary organic aerosol. *Atmospheric Chemistry and Physics, 9*(3), 795-812.

Asa-Awuku, A., Miracolo, M. A., Kroll, J. H., Robinson, A. L., & Donahue, N. M. (2009). Mixing and phase partitioning of primary and secondary organic aerosols. *Geophysical Research Letters, 36*(15). doi:Artn L1582710.1029/2009gl039301

Asa-Awuku, A., Moore, R. H., Nenes, A., Bahreini, R., Holloway, J. S., Brock, C. A., . . . Huey, L. G. (2011). Airborne cloud condensation nuclei measurements during the 2006 Texas Air Quality Study. *Journal of Geophysical Research-Atmospheres, 116*(D11). doi:Artn D1120110.1029/2010jd014874

Asa-Awuku, A., Nenes, A., Gao, S., Flagan, R. C., & Seinfeld, J. H. (2010). Water-soluble SOA from Alkene ozonolysis: composition and droplet activation kinetics inferences from analysis of CCN activity. *Atmospheric Chemistry and Physics, 10*(4), 1585-1597.

Bond, T. C., Doherty, S. J., Fahey, D. W., Forster, P. M., Berntsen, T., DeAngelo, B. J., . . . Zender, C. S. (2013). Bounding the role of black carbon in the climate system: A scientific assessment. *Journal of Geophysical Research-Atmospheres, 118*(11), 5380-5552. doi:10.1002/jgrd.50171

Bougiatioti, A., Fountoukis, C., Kalivitis, N., Pandis, S. N., Nenes, A., & Mihalopoulos, N. (2009). Cloud condensation nuclei measurements in the marine boundary layer of the eastern Mediterranean: CCN closure and droplet growth kinetics. *Atmospheric Chemistry and Physics, 9*(18), 7053-7066.

Canagaratna, M. R., Jayne, J. T., Jimenez, J. L., Allan, J. D., Alfarra, M. R., Zhang, Q., . . . Worsnop, D. R. (2007). Chemical and microphysical characterization of ambient aerosols with the aerodyne aerosol mass spectrometer. *Mass Spectrom Rev, 26*(2), 185-222. doi:10.1002/mas.20115

Cappa, C. D., Onasch, T. B., Massoli, P., Worsnop, D. R., Bates, T. S., Cross, E. S., . . . Zaveri, R. A. (2012). Radiative Absorption Enhancements Due to the Mixing State of Atmospheric Black Carbon. *Science, 337*(6098), 1078-1081. doi:10.1126/science.1223447

Chan, M., & Chan, C. K. (2005). Mass transfer effects in hygroscopic measurements of aerosol particles. *Atmospheric Chemistry and Physics, 5*(10), 2703-2712.

Chan, M. N., & Chan, C. K. (2007). Mass transfer effects on the hygroscopic growth of ammonium sulfate particles with a water-insoluble coating. *Atmospheric Environment, 41*(21), 4423-4433. doi:10.1016/j.atmosenv.2007.01.047

Chan, T. W., Meloche, E., Kubsh, J., & Brezny, R. (2014). Black carbon emissions in gasoline exhaust and a reduction alternative with a gasoline particulate filter. *Environ Sci Technol, 48*(10), 6027-6034. doi:10.1021/es501791b

Chan, T. W., Meloche, E., Kubsh, J., Rosenblatt, D., Brezny, R., & Rideout, G. (2012). Evaluation of a gasoline particulate filter to reduce particle emissions from a gasoline direct injection vehicle. *SAE International Journal of Fuels and Lubricants, 5*(2012-01-1727), 1277-1290.

Chang, R. Y. W., Slowik, J. G., Shantz, N. C., Vlasenko, A., Liggio, J., Sjostedt, S. J., . . . Abbatt, J. P. D. (2010). The hygroscopicity parameter (kappa) of ambient organic aerosol at a field site subject to biogenic and anthropogenic influences: relationship to degree of aerosol oxidation. *Atmospheric Chemistry and Physics, 10*(11), 5047-5064. doi:10.5194/acp-10-5047-2010

Chirico, R., DeCarlo, P., Heringa, M., Tritscher, T., Richter, R., Prévôt, A., . . . Gysel, M. (2010). Impact of aftertreatment devices on primary emissions and secondary organic aerosol formation potential from in-use diesel vehicles: results from smog chamber experiments. *Atmospheric Chemistry and Physics, 10*(23), 11545.

Cocker, D. R., 3rd, Flagan, R. C., & Seinfeld, J. H. (2001). State-of-the-art chamber facility for studying atmospheric aerosol chemistry. *Environ Sci Technol, 35*(12), 2594-2601.

Cubison, M., Ervens, B., Feingold, G., Docherty, K., Ulbrich, I., Shields, L., . . . Jimenez, J. (2008). The influence of chemical composition and mixing state of Los Angeles urban aerosol on CCN number and cloud properties. *Atmospheric Chemistry and Physics, 8*(18), 5649-5667.

DeCarlo, P. F., Slowik, J. G., Worsnop, D. R., Davidovits, P., & Jimenez, J. L. (2004). Particle morphology and density characterization by combined mobility and aerodynamic diameter measurements. Part 1: Theory. *Aerosol Science and Technology, 38*(12), 1185-1205. doi:10.1080/027868290903907

Duplissy, J., DeCarlo, P. F., Dommen, J., Alfarra, M. R., Metzger, A., Barmpadimos, I., . . . Baltensperger, U. (2011). Relating hygroscopicity and composition of organic aerosol particulate matter. *Atmospheric Chemistry and Physics, 11*(3), 1155-1165. doi:10.5194/acp-11-1155-2011

Dusek, U., Frank, G., Curtius, J., Drewnick, F., Schneider, J., Kürten, A., . . . Pöschl, U. (2010). Enhanced organic mass fraction and decreased hygroscopicity of cloud condensation nuclei (CCN) during new particle formation events. *Geophysical Research Letters, 37*(3).

Dusek, U., Frank, G., Massling, A., Zeromskiene, K., Iinuma, Y., Schmid, O., . . . Andreae, M. (2011). Water uptake by biomass burning aerosol at sub-and supersaturated conditions: closure studies and implications for the role of organics. *Atmospheric Chemistry and Physics, 11*(18), 9519-9532.

Dusek, U., Frank, G. P., Hildebrandt, L., Curtius, J., Schneider, J., Walter, S., . . . Andreae, M. O. (2006). Size matters more than chemistry for cloud-nucleating ability of aerosol particles. *Science, 312*(5778), 1375-1378. doi:10.1126/science.1125261

Ellies, B., Schenk, C., & Dekraker, P. (2016). *Benchmarking and Hardware-in-the-Loop Operation of a 2014 MAZDA SkyActiv 2.0 L 13: 1 Compression Ratio Engine* (0148-7191). Retrieved from

Engelhart, G., Asa-Awuku, A., Nenes, A., & Pandis, S. (2008). CCN activity and droplet growth kinetics of fresh and aged monoterpene secondary organic aerosol. *Atmospheric Chemistry and Physics, 8*(14), 3937-3949.

Engelhart, G. J., Moore, R. H., Nenes, A., & Pandis, S. N. (2011). Cloud condensation nuclei activity of isoprene secondary organic aerosol. *Journal of Geophysical Research: Atmospheres, 116*(D2).

EPA. (2012). 2017 and later model year light-duty vehicle greenhouse gas emissions and corporate average fuel economy standards; final rule. *Federal Register, 77*(199), 62623-63200.

Fofie, E. A., Castellucio, V., & Asa-Awuku, A. (2017). Exploring CCN droplet kinetics with a higher sensitivity optical particle counter *Aerosol Sci Technol, in review*.

Fofie, E. A., Donahue, N. M., & Asa-Awuku, A. (2017). Cloud condensation nuclei activity and droplet formation of primary and secondary organic aerosol mixtures *Aerosol Sci Technol, under review*

Frosch, M., Bilde, M., DeCarlo, P., Juranyi, Z., Tritscher, T., Dommen, J., . . . Baltensperger, U. (2011). Relating cloud condensation nuclei activity and oxidation level of α-pinene secondary organic aerosols. *Journal of Geophysical Research: Atmospheres, 116*(D22).

Giordano, M., Espinoza, C., & Asa-Awuku, A. (2015). Experimentally measured morphology of biomass burning aerosol and its impacts on CCN ability. *Atmospheric Chemistry and Physics, 15*(4), 1807-1821. doi:10.5194/acp-15-1807-2015

Giordano, M. R., Chong, J., Weise, D. R., & Asa-Awuku, A. A. (2016). Does chronic nitrogen deposition during biomass growth affect atmospheric emissions from biomass burning? *Environmental Research Letters, 11*(3), 034007.

Gunthe, S., King, S., Rose, D., Chen, Q., Roldin, P., Farmer, D., . . . Martin, S. (2009). Cloud condensation nuclei in pristine tropical rainforest air of Amazonia: size-resolved measurements and modeling of atmospheric aerosol composition and CCN activity. *Atmospheric Chemistry and Physics, 9*(19), 7551-7575.

Gysel, M., McFiggans, G., & Coe, H. (2009). Inversion of tandem differential mobility analyser (TDMA) measurements. *Journal of Aerosol Science, 40*(2), 134-151.

Huff Hartz, K. E., Rosenørn, T., Ferchak, S. R., Raymond, T. M., Bilde, M., Donahue, N. M., & Pandis, S. N. (2005). Cloud condensation nuclei activation of monoterpene and sesquiterpene secondary organic aerosol. *Journal of Geophysical Research: Atmospheres, 110*(D14).

Hula, A., Bunker, A., & Alson, J. (2015). *Light-Duty Automotive Technology, Carbon Dioxide Emissions, and Fuel Economy Trends: 1975 Through 2015*. Retrieved from

Iwamoto, Y., Noma, K., Nakayama, O., Yamauchi, T., & Ando, H. (1997). *Development of gasoline direct injection engine* (0148-7191). Retrieved from

Jacobson, M. Z. (2001). Strong radiative heating due to the mixing state of black carbon in atmospheric aerosols. *Nature, 409*(6821), 695-697.

Jimenez, J., Canagaratna, M., Donahue, N., Prevot, A., Zhang, Q., Kroll, J. H., . . . Ng, N. (2009). Evolution of organic aerosols in the atmosphere. *Science, 326*(5959), 1525-1529.

Karavalakis, G., Short, D., Vu, D., Villela, M., Asa-Awuku, A., & Durbin, T. D. (2014). Evaluating the regulated emissions, air toxics, ultrafine particles, and black carbon from SI-PFI and SI-DI vehicles operating on different ethanol and iso-butanol blends. *Fuel, 128*, 410-421. doi:10.1016/j.fuel.2014.03.016

Khalizov, A. F., Lin, Y., Qiu, C., Guo, S., Collins, D., & Zhang, R. (2013). Role of OH-initiated oxidation of isoprene in aging of combustion soot. *Environmental science & technology, 47*(5), 2254-2263.

Khvorostyanov, V. I., & Curry, J. A. (2007). Refinements to the Köhler's theory of aerosol equilibrium radii, size spectra, and droplet activation: Effects of humidity and insoluble fraction. *Journal of Geophysical Research: Atmospheres, 112*(D5).

King, S. M., Rosenoern, T., Shilling, J. E., Chen, Q., & Martin, S. T. (2009). Increased cloud activation potential of secondary organic aerosol for atmospheric mass loadings. *Atmospheric Chemistry and Physics, 9*(9), 2959-2971.

Köhler, H. (1936). The nucleus in and the growth of hygroscopic droplets. *Transactions of the Faraday Society, 32*, 1152-1161.

Kreidenweis, S., & Asa-Awuku, A. (2014). 5.13-Aerosol hygroscopicity: Particle water content and its role in atmospheric processes.

Lamarque, J. F., Bond, T. C., Eyring, V., Granier, C., Heil, A., Klimont, Z., . . . Owen, B. (2010). Historical (1850–2000) gridded anthropogenic and biomass burning emissions of reactive gases and aerosols: methodology and application. *Atmospheric Chemistry and Physics, 10*(15), 7017-7039.

Lance, S., Nenes, A., Mazzoleni, C., Dubey, M. K., Gates, H., Varutbangkul, V., . . . Flagan, R. C. (2009). Cloud condensation nuclei activity, closure, and droplet growth kinetics of Houston aerosol during the Gulf of Mexico Atmospheric Composition and Climate Study (GoMACCS). *Journal of Geophysical Research: Atmospheres, 114*(D7).

Lance, S., Nenes, A., Medina, J., & Smith, J. N. (2006). Mapping the Operation of the DMT Continuous Flow CCN Counter. *Aerosol Science and Technology, 40*(4), 242-254. doi:10.1080/02786820500543290

Lance, S., Raatikainen, T., Onasch, T. B., Worsnop, D. R., Yu, X.-Y., Alexander, M., . . . Nenes, A. (2013). Aerosol mixing state, hygroscopic growth and cloud activation efficiency during MIRAGE 2006. *Atmospheric Chemistry and Physics, 13*(9), 5049-5062.

Laskina, O., Morris, H. S., Grandquist, J. R., Qin, Z., Stone, E. A., Tivanski, A. V., & Grassian, V. H. (2015). Size matters in the water uptake and hygroscopic growth of atmospherically relevant multicomponent aerosol particles. *The Journal of Physical Chemistry A, 119*(19), 4489-4497.

Lathem, T. L., & Nenes, A. (2011). Water Vapor Depletion in the DMT Continuous-Flow CCN Chamber: Effects on Supersaturation and Droplet Growth. *Aerosol Science and Technology, 45*(5), 604-615. doi:10.1080/02786826.2010.551146

Ma, X., Zangmeister, C. D., Gigault, J., Mulholland, G. W., & Zachariah, M. R. (2013). Soot aggregate restructuring during water processing. *Journal of Aerosol Science, 66*, 209-219.

Malloy, Q. G., Nakao, S., Qi, L., Austin, R., Stothers, C., Hagino, H., & Cocker III, D. R. (2009). Real-time aerosol density determination utilizing a modified scanning mobility particle sizer—aerosol particle mass analyzer system. *Aerosol Science and Technology, 43*(7), 673-678.

Maricq, M. M., Szente, J. J., & Jahr, K. (2012). The impact of ethanol fuel blends on PM emissions from a light-duty GDI vehicle. *Aerosol Science and Technology, 46*(5), 576-583.

Massoli, P., Lambe, A., Ahern, A., Williams, L., Ehn, M., Mikkilä, J., . . . Jayne, J. (2010). Relationship between aerosol oxidation level and hygroscopic properties of laboratory generated secondary organic aerosol (SOA) particles. *Geophysical Research Letters, 37*(24).

Mikhailov, E., Vlasenko, S., Martin, S., Koop, T., & Pöschl, U. (2009). Amorphous and crystalline aerosol particles interacting with water vapor: conceptual framework and experimental evidence for restructuring, phase transitions and kinetic limitations. *Atmospheric Chemistry and Physics, 9*(24), 9491-9522.

Modini, R. L., Johnson, G. R., He, C., & Ristovski, Z. D. (2010). Observation of the suppression of water uptake by marine particles. *Atmospheric Research, 98*(2), 219-228.

Moffet, R. C., & Prather, K. A. (2009). In-situ measurements of the mixing state and optical properties of soot with implications for radiative forcing estimates. *Proceedings of the National Academy of Sciences, 106*(29), 11872-11877.

Moore, R. H., Nenes, A., & Medina, J. (2010). Scanning Mobility CCN Analysis—A Method for Fast Measurements of Size-Resolved CCN Distributions and Activation Kinetics. *Aerosol Science and Technology, 44*(10), 861-871. doi:10.1080/02786826.2010.498715

Nakao, S., Shrivastava, M., Nguyen, A., Jung, H., & Cocker III, D. (2011). Interpretation of secondary organic aerosol formation from diesel exhaust photooxidation in an environmental chamber. *Aerosol Science and Technology, 45*(8), 964-972.

Noziere, B. (2016). Don't forget the surface. *Science, 351*(6280), 1396-1397.

Padró, L. T., Tkacik, D., Lathem, T., Hennigan, C. J., Sullivan, A. P., Weber, R. J., . . . Nenes, A. (2010). Investigation of cloud condensation nuclei properties and droplet growth kinetics of the water-soluble aerosol fraction in Mexico City. *Journal of Geophysical Research: Atmospheres, 115*(D9).

Petters, M. D., Carrico, C. M., Kreidenweis, S. M., Prenni, A. J., DeMott, P. J., Collett, J. L., & Moosmueller, H. (2009). Cloud condensation nucleation activity of biomass burning aerosol. *Journal of Geophysical Research: Atmospheres, 114*(D22).

Petters, M. D., & Kreidenweis, S. M. (2007). A single parameter representation of hygroscopic growth and cloud condensation nucleus activity. *Atmospheric Chemistry and Physics, 7*(8), 1961-1971.

Petters, M. D., & Kreidenweis, S. M. (2008). A single parameter representation of hygroscopic growth and cloud condensation nucleus activity–Part 2: Including solubility. *Atmospheric Chemistry and Physics, 8*(20), 6273-6279.

Piock, W., Hoffmann, G., Berndorfer, A., Salemi, P., & Fusshoeller, B. (2011). Strategies towards meeting future particulate matter emission requirements in homogeneous gasoline direct injection engines. *SAE International Journal of Engines, 4*(2011-01-1212), 1455-1468.

Pöschl, U., Martin, S., Sinha, B., Chen, Q., Gunthe, S., Huffman, J., . . . Helas, G. (2010). Rainforest aerosols as biogenic nuclei of clouds and precipitation in the Amazon. *Science, 329*(5998), 1513-1516.

Prenni, A. J., DeMott, P. J., Kreidenweis, S. M., Sherman, D. E., Russell, L. M., & Ming, Y. (2001). The effects of low molecular weight dicarboxylic acids on cloud formation. *The Journal of Physical Chemistry A, 105*(50), 11240-11248.

Prenni, A. J., Petters, M. D., Kreidenweis, S. M., DeMott, P. J., & Ziemann, P. J. (2007). Cloud droplet activation of secondary organic aerosol. *Journal of Geophysical Research: Atmospheres, 112*(D10).

Presto, A., Gordon, T., & Robinson, A. (2014). Primary to secondary organic aerosol: evolution of organic emissions from mobile combustion sources. *Atmospheric Chemistry and Physics, 14*(10), 5015-5036.

Pruppacher, H., & Klett, J. (1997). Microphysics of Clouds and Precipitation: With an Introduction to Cloud Chemistry and Cloud Electricity, 954 pp: Springer, New York

Qi, L., Nakao, S., Tang, P., & Cocker III, D. (2010). Temperature effect on physical and chemical properties of secondary organic aerosol from m-xylene photooxidation. *Atmospheric Chemistry and Physics, 10*(8), 3847-3854.

Rader, D., & McMurry, P. (1986). Application of the tandem differential mobility analyzer to studies of droplet growth or evaporation. *Journal of Aerosol Science, 17*(5), 771-787.

Ramanathan, V., & Carmichael, G. (2008). Global and regional climate changes due to black carbon. *Nature geoscience, 1*(4), 221-227.

Riemer, N., Vogel, H., & Vogel, B. (2004). Soot aging time scales in polluted regions during day and night. *Atmospheric Chemistry and Physics, 4*(7), 1885-1893.

Riipinen, I., Rastak, N., & Pandis, S. (2015). Connecting the solubility and CCN activation of complex organic aerosols: a theoretical study using solubility distributions. *Atmospheric Chemistry and Physics, 15*(11), 6305-6322.

Rissler, J., Messing, M. E., Malik, A. I., Nilsson, P. T., Nordin, E. Z., Bohgard, M., . . . Pagels, J. H. (2013). Effective density characterization of soot agglomerates from various sources and comparison to aggregation theory. *Aerosol Science and Technology, 47*(7), 792-805.

Robinson, E. S., Donahue, N. M., Ahern, A. T., Ye, Q., & Lipsky, E. (2016). Single-particle measurements of phase partitioning between primary and secondary organic aerosols. *Faraday discussions*.

Rose, D., Gunthe, S. S., Mikhailov, E., Frank, G. P., Dusek, U., Andreae, M. O., & Pöschl, U. (2008). Calibration and measurement uncertainties of a continuous-flow cloud condensation nuclei counter (DMT-CCNC): CCN activation of ammonium sulfate and sodium chloride aerosol particles in theory and experiment. *Atmospheric Chemistry and Physics, 8*(5), 1153-1179.

Ruehl, C., Chuang, P., Nenes, A., Cappa, C., Kolesar, K., & Goldstein, A. (2012). Strong evidence of surface tension reduction in microscopic aqueous droplets. *Geophysical Research Letters, 39*(23).

Ruehl, C. R., Chuang, P. Y., & Nenes, A. (2008). How quickly do cloud droplets form on atmospheric particles? *Atmospheric Chemistry and Physics, 8*(4), 1043-1055.

Ruehl, C. R., Davies, J. F., & Wilson, K. R. (2016). An interfacial mechanism for cloud droplet formation on organic aerosols. *Science, 351*(6280), 1447-1450. doi:10.1126/science.aad488910.1126/science.aad4889.

Sasser, E., Hemby, J., Adler, K., Anenberg, S., Bailey, C., Brockman, L., . . . Dawson, J. (2012). Report to Congress on Black Carbon. *Department of the Interior, Environment, and Related Agencies*.

Schwarz, J. P., Gao, R. S., Fahey, D. W., Thomson, D. S., Watts, L. A., Wilson, J. C., . . . Aikin, K. C. (2006). Single-particle measurements of midlatitude black carbon and light-scattering aerosols from the boundary layer to the lower stratosphere. *Journal of Geophysical Research, 111*(D16). doi:10.1029/2006jd007076

Seinfeld, J. H., & Pandis, S. N. (2006). Atmospheric Chemistry and Physics, A Wiley-Inter Science Publication: John Wiley & Sons Inc, New York

Shantz, N., Chang, R.-W., Slowik, J., Vlasenko, A., Abbatt, J., & Leaitch, W. (2010). Slower CCN growth kinetics of anthropogenic aerosol compared to biogenic aerosol observed at a rural site. *Atmospheric Chemistry and Physics, 10*(1), 299-312.

Smith, M., Bertram, A., & Martin, S. (2012). Deliquescence, efflorescence, and phase miscibility of mixed particles of ammonium sulfate and isoprene-derived secondary organic material. *Atmospheric Chemistry and Physics, 12*(20), 9613-9628.

Spracklen, D., Carslaw, K., Pöschl, U., Rap, A., & Forster, P. (2011). Global cloud condensation nuclei influenced by carbonaceous combustion aerosol. *Atmospheric Chemistry and Physics, 11*(17), 9067-9087.

Suda, S. R., Petters, M., Matsunaga, A., Sullivan, R., Ziemann, P., & Kreidenweis, S. (2012). Hygroscopicity frequency distributions of secondary organic aerosols. *Journal of Geophysical Research: Atmospheres, 117*(D4).

Tritscher, T., Jurányi, Z., Martin, M., Chirico, R., Gysel, M., Heringa, M. F., . . . Weingartner, E. (2011). Changes of hygroscopicity and morphology during ageing of diesel soot. *Environmental Research Letters, 6*(3), 034026.

Vaden, T. D., Song, C., Zaveri, R. A., Imre, D., & Zelenyuk, A. (2010). Morphology of mixed primary and secondary organic particles and the adsorption of spectator organic gases during aerosol formation. *Proceedings of the National Academy of Sciences, 107*(15), 6658-6663.

Vu, D., Short, D., Karavalakis, G., Durbin, T., & Asa-Awuku, A. (2015). Integrating Cloud Condensation Nuclei Predictions with Fast Time Resolved Aerosol Instrumentation to Determine the Hygroscopic Properties of Emissions Over Transient Drive Cycles. *Aerosol Science and Technology, 49*(11), 1149-1159.

Vu, D., Short, D. Z., Karavalakis, G., Durbin, T. D., & Asa-Awuku, A. (2017). Will Aerosol Hygroscopicity Change with Biodiesel, Renewable Diesel Fuels and Emission Control Technologies? *Environmental science & technology*.

Wang, C., Xu, H., Herreros, J. M., Wang, J., & Cracknell, R. (2014). Impact of fuel and injection system on particle emissions from a GDI engine. *Applied Energy, 132*, 178-191.

Wang, J., Cubison, M., Aiken, A., Jimenez, J., & Collins, D. (2010). The importance of aerosol mixing state and size-resolved composition on CCN concentration and the variation of the importance with atmospheric aging of aerosols. *Atmospheric Chemistry and Physics, 10*(15), 7267-7283.

Whitaker, P., Kapus, P., Ogris, M., & Hollerer, P. (2011). Measures to reduce particulate emissions from gasoline DI engines. *SAE International Journal of Engines, 4*(2011-01-1219), 1498-1512.

Whitehead, J., Irwin, M., Allan, J., Good, N., & McFiggans, G. (2014). A meta-analysis of particle water uptake reconciliation studies. *Atmospheric Chemistry and Physics, 14*(21), 11833-11841.

Wittbom, C., Eriksson, A., Rissler, J., Carlsson, J., Roldin, P., Nordin, E., . . . Svenningsson, B. (2014). Cloud droplet activity changes of soot aerosol upon smog chamber ageing. *Atmospheric Chemistry and Physics, 14*(18), 9831-9854.

Xing, J., Pleim, J., Mathur, R., Pouliot, G., Hogrefe, C., Gan, C.-M., & Wei, C. (2013). Historical gaseous and primary aerosol emissions in the United States from 1990 to 2010. *Atmospheric Chemistry and Physics, 13*(15), 7531-7549.

Yi, J., Wooldridge, S., Coulson, G., Hilditch, J., Iyer, C. O., Moilanen, P., . . . VanDerWege, B. (2009). Development and optimization of the Ford 3.5 L V6 EcoBoost combustion system. *SAE International Journal of Engines, 2*(2009-01-1494), 1388-1407.

Zaveri, R. A., Barnard, J. C., Easter, R. C., Riemer, N., & West, M. (2010). Particle-resolved simulation of aerosol size, composition, mixing state, and the associated optical and cloud condensation nuclei activation properties in an evolving urban plume. *Journal of Geophysical Research: Atmospheres, 115*(D17).

Zhang, J., Fan, X., Graham, L., Chan, T. W., & Brook, J. R. (2012). Evaluation of an annular denuder system for carbonaceous aerosol sampling of diesel engine emissions. *http://dx.doi.org/10.1080/10962247.2012.739582*. doi:J. Air & Waste Manage. Assoc., Vol. 63, No. 1, January 2013: pp. 87–99

Zhao, D., Buchholz, A., Kortner, B., Schlag, P., Rubach, F., Fuchs, H., . . . Watne, Å. (2016). Cloud condensation nuclei activity, droplet growth kinetics, and hygroscopicity of biogenic and anthropogenic secondary organic aerosol (SOA). *Atmospheric Chemistry and Physics, 16*(2), 1105-1121.